Electronic Supplementary Material (ESI) for Journal of Materials Chemistry A.
This journal is © The Royal Society of Chemistry 2024

# Supporting Information

## Potassium Ferrite Nanosheets with Tin Doping for Enhanced Large-Current-Density $H_2$ Production and Ultra-Long Life Rechargeable Zn-Air Battery

Juan Jian,[a] Zhuo Wang,[a] Yu Qiao,[a] Fen Yao,[a] Meiting Wang,[a] Limin Chang[a,*] and Ping Nie[a,*]

[a] Key Laboratory of Preparation and Applications of Environmental Friendly Material of the Ministry of Education, College of Chemistry, Jilin Normal University, Changchun 130103, P. R. China

* Corresponding authors' E-mails: changlimin2139@163.com; xdnieping2009@sina.com

## 1. Material and Experimental Instruments

### 1.1 Materials used in the experiment

Pt/C (20 wt%) was obtained from Macklin Ltd. (Shanghai, China), $RuO_2$ was synthesized from ruthenium chloride hydrate ($RuCl_3 \cdot xH_2O$) purchased from Aladdin Ltd. (Shanghai, China).[1] Nickel foam (NF) was provided by the Li Yuan Technology Co. Ltd. (Shanxi, China). KOH, $Fe(NO_3)_3 \cdot 9H_2O$, $Na_2SnO_3 \cdot 3H_2O$, HCl and other chemicals are supplied by the Beijing Chemical Reagents Company. Apart from the NF, all the chemicals are analytical pure and do not needed further purification.

### 1.2 Experimental Section

***Basic Phase Characterizations***

X-ray diffraction (XRD) experiment was tested on a Rigaku D-Max 2550 diffractometer with Cu-Kα radiation (λ = 1.5418 Å). Scanning electron microscope (SEM) and energy dispersive X-ray spectroscopy (EDX) images were obtained on a JEOL-6700 scanning electron microscope. Transmission electron microscope (TEM), high resolution TEM (HRTEM) images were obtained with microscopy of Philips-FEI Tecnai G2S-Twin, equipped with a field emission gun operating at 200 kV. X-ray photoelectron spectra (XPS) analysis was performed on a VG Scienta R3000 spectrometer with Al Kα (1486.6 eV) as the X-ray source. Contact angle (CA) experiment was analyzed by the machine of Dataphysics OCA20 at room temperature.

***Electrochemical Measurements***

The electrochemical measurements were conducted using the three-electrode system with the electrochemical workstation (CHI 760e). The as-prepared electrodes were directly used as the working electrodes; meanwhile, graphite rod and Hg/HgO electrode were served as counter and reference electrodes, respectively. 1.0 M KOH solution was used as

electrolyte for HER, OER and OWS devices, while 0.1 M KOH were applied for the ORR process. Potentials were normalized versus the standard hydrogen electrode (RHE) according to formula below:

$$E_{(RHE)} = E_{(Hg/HgO)} + 0.098\ V + 0.0591\ pH \quad (1)$$

Here, "$E_{(Hg/HgO)}$" is the potential we directly measured during the experiment.

Polarization curves were performed via sweeping potentials at a scan rate of 2.0 mV $s^{-1}$. The measured potentials were calibrated with *iR* compensation. Corresponding stability data were examined through current-time curves at the constant potentials.

The loading was calculated through a series of parallel experiments, the mass changes of NF-based materials before and after the synthesis reaction were used to determine the loading capacity.

**Tafel slope:**

The data of Tafel slope can be plotted by the gained linear sweep voltammetry (LSV) curves, which is obtained from the follow equation:

$$\eta = a + b \log j \quad (2)$$

Where, "η" refers to the overpotential; "j" is the current density; "a" relates to the $j_0$ (exchange current density) and can be reflected by the intercept; "b" is the Tafel slope we need to acquire.

**Electrochemical surface area (ECSA)**

The ECSA is calculated by the formula below:

$$ECSA = A * C_{dl} / C_s \quad (3)$$

Where "A" refers to the area of the working electrode, and we set the electrode area to 0.25 $cm^2$ throughout the electrocatalytic water splitting testing; "$C_s$" relates to the electrolyte and $C_s$ = 0.04 mF $cm^{-2}$, "$C_{dl}$" is the abbreviation of double layer capacitance and

calculated from a series of CV curves that tested within the non-Faraday potential range (0.9254-1.0254 V vs. RHE), scan rate changed from 10 to 100 mV $s^{-1}$, increased with 10 mV $s^{-1}$ each time.

**Faraday efficiency (FE):**

Faraday efficiency (FE) of Sn-KFO for OER/HER can be calculated by the ratio of the amount of $O_2/H_2$ collected by drainage method and the theoretical $O_2/H_2$. Take OER for example, the actual amount $O_2$ production (labeled as $n_{o\text{-experimental}}$) can be calculated using the equation of $n_{o\text{-experimental}} = V/V_m$, where V is the volume of $O_2$ collected from the chronoamperometry testing; $V_m$ is molar volume of ideal gas, and $V_m$ = 22.4 L $mol^{-1}$. For the theoretical $O_2$ (marked as $n_{o\text{-theoretical}}$) accumulated during the OER. According the OER equation of $4OH^- \rightarrow O_2 + 2H_2O + 4e^-$, where, the electrolytic efficiency (η) can be measured by the equation of η = z*n*F/Q. Here, "n" is the mole of $O_2$ generated during the OER, and can be marked as $n_{o\text{-theoretical}}$; "z" is the number of transferred electrons generated per mole of $O_2$ during the OER, here, z = 4; "F" is the Faraday constant, F = 96485 C $mol^{-1}$; "Q" refers to the actual quantity of electric charge, and can be calculated by the flume of Q = $\Sigma$i*t. In the chronoamperometry experiment, the Q can be directly calculated. To evaluate the FE of a catalyst for OER, we assume that 100 % current efficiency occurs during the whole reaction. Hence, $1 = 4*F*n_{o\text{-theoretical}}/Q$, therefore, $n_{o\text{-theoretical}} = Q/(4*F)$. The calculation of FE for HER is similar with the OER, merely the the number of transferred electrons generated per mole of $H_2$ during the HER is 2.

***Assembly and Testing of the Zn-Air Battery***

As for the liquid Zn-air battery, in order to avoid electrolyte leakage, we physically compounded the NF-based catalyst with the waterproof/breathable carbon film, and then assembled the complex as the air-cathode of the Zn-air battery.

Both the charge and discharge curves were measured by the CHI 760e, the power density was calculated from the data of the discharge curve. Charge-discharge curves at current density of 10 mA $cm^{-2}$ in this work were measured by the Land battery test system.

## 2. Theoretical Section

### *Computation Details*

The KFO is a new 3D open-framework ferrite, which belongs to the trigonal space group $P\bar{3}1m$, and the optimized unit cell parameters are a = b = 5.006 Å and c = 6.633 Å, all of which are very close to the corresponding experimental values (a = b = 5.155 and c = 6.902 Å).[2] First-principles calculations were carried out using density functional theory (DFT) with generalized gradient approximation (GGA) of Perdew-Burke-Ernzerhof (PBE) implemented in the Vienna Ab-Initio Simulation Package (VASP).[3] The valence electronic states were expanded on the basis of plane waves with the core-valence interaction represented using the projector augmented plane wave (PAW) approach and a cutoff of 520 eV.[4] A 1.75 layered (001) facet was cleaved with the vacuum slab height of 20 Å. A 3 × 3 supercell containing 117 O, 18 K and 72 Fe atoms were studied. To model the substitution, a Fe atom in octahedral coordination was replaced by a Sn atom, and can be modeled by the corresponding slab (Fig. S11). A Γ-centered k-mesh of 2 × 2 × 1 was used for the Fe-O surface calculations. During the computational process, the outermost Fe-O layer in the theoretical slab model is fully relaxed without any symmetry or direction restrictions, while the remaining atoms are kept frozen.

The adsorption energy of H was calculated based on the following equation:

$$\Delta E = E_{slab\text{-}H} - 0.5E_{H2} - E_{slab} \quad (4)$$

Where, $E_{slab\text{-}H}$, $E_{H2}$, and $E_{slab}$ are the total energy of the whole system, the $H_2$ molecule, and the slab, respectively.

Then, the reaction free energy change can be obtained from equation below:

$$\Delta G = \Delta E + \Delta ZPE - T\Delta S \quad (5)$$

Here, the difference in zero-point energies, ΔZPE, and the change in entropy Δ*S* are determined by using DFT-calculated vibrational frequencies and standard tables for the gas-phase molecule.[5]

## 3. Supplementary Figures and Tables

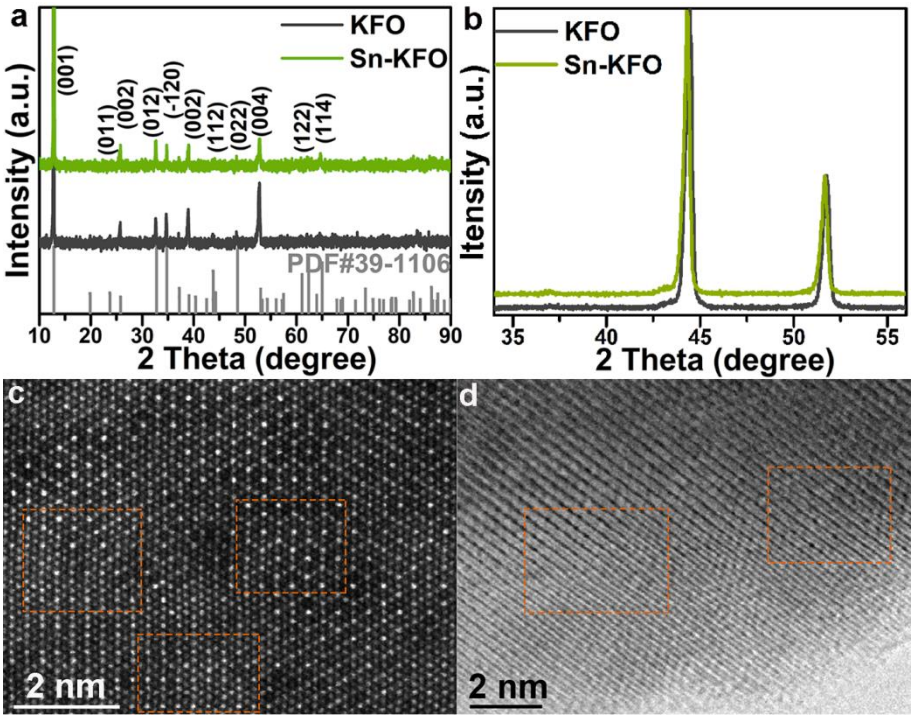


**Fig. S1**. The XRD results of (a) KFO powder and Sn-KFO powder, (b) enlarged patterns of NF based KFO and Sn-KFO. (c, d) The AC HADDF-STEM images of the Sn-KFO.

Obviously, the patterns of Sn-KFO powder illustrated in Fig. S1a is well consistent with that of the pure KFO powder. This confirms that the as synthesized NF based catalyst is the KFO-based material. As shown in Fig. S1b, comparing with the pure KFO, the XRD pattern of Sn-KFO displayed a slightly low degree shift, which mainly attribute to the introduction of Sn. Additionally, the AC HADDF-STEM images displayed in Fig. S1c,d also confirm the slight change in lattice spacing after the Sn-doping.

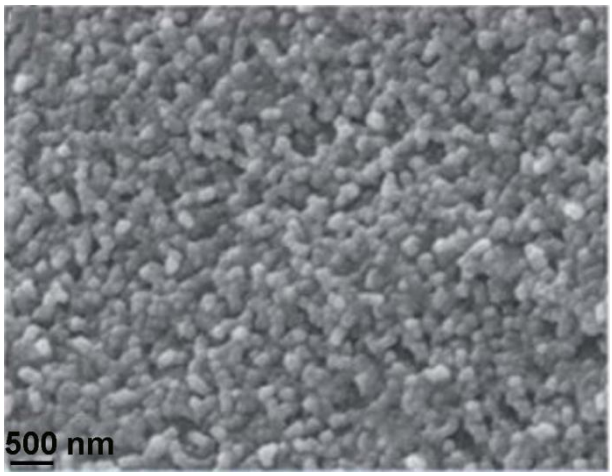


**Fig. S2**. The SEM image of pure KFO.

**Table S1.** $C_{dl}$, ECSA and related data of KFO and Sn-KFO.

| Catalyst | $C_{dl}$ (mF cm$^{-2}$) | $C_s$ (mF cm$^{-2}$) | A (cm$^2$) | ECSA (cm$^2$) |
|---|---|---|---|---|
| **KFO** | 3.25 | 0.04 | 0.25 | 20.31 |
| **Sn-KFO** | 3.95 | 0.04 | 0.25 | 24.69 |

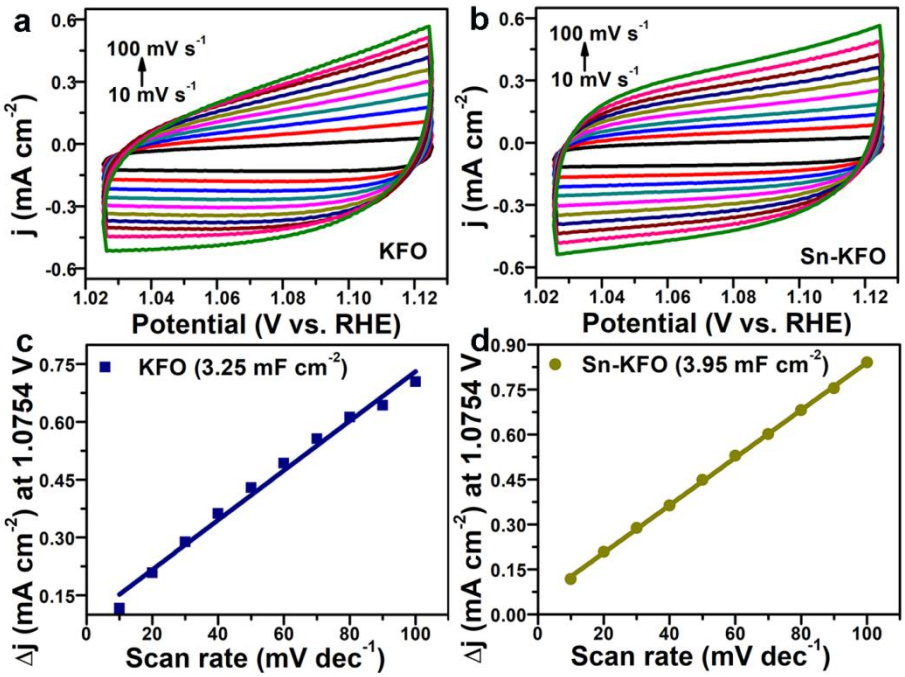


**Fig. S3.** The CV curves at different scan rate of (a) KFO, (b) Sn-KFO, and (c, d) their corresponding relationships between scan rate and Δj = 1.0754 V.

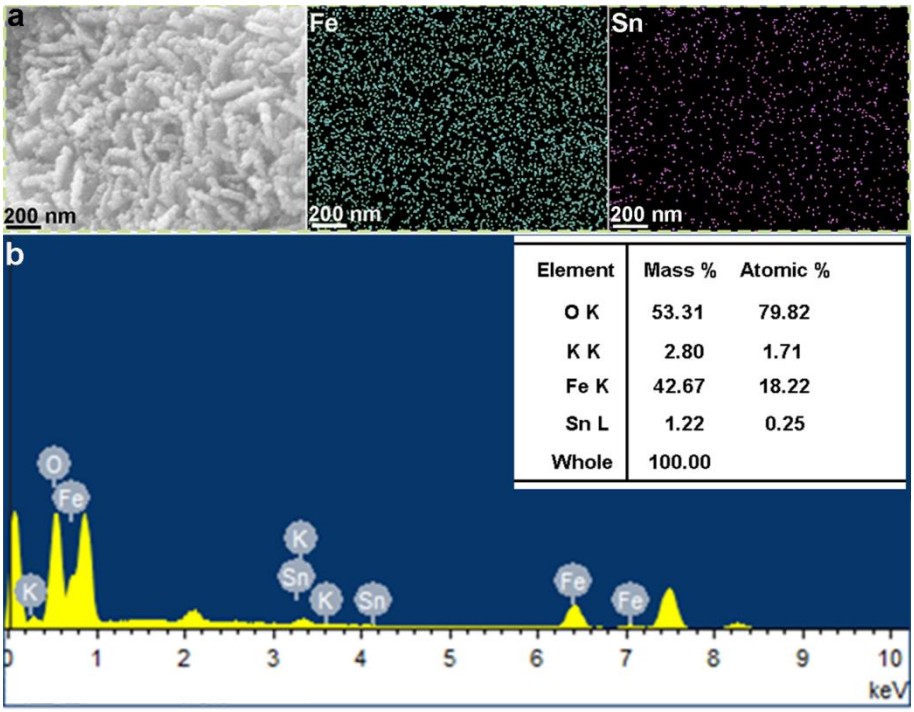


**Fig. S4.** SEM-mapping and corresponding content of constituent elements of Sn-KFO.

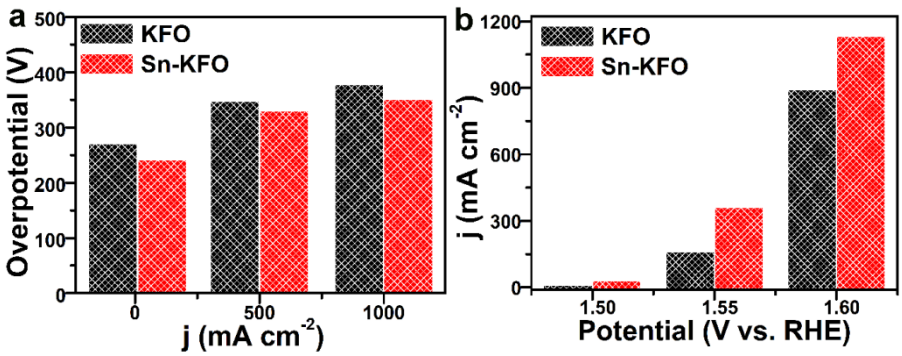


**Fig. S5**. (a, b) The bar-graphs between current density (j) and potential (V) of Sn-KFO and KFO during the OER process.

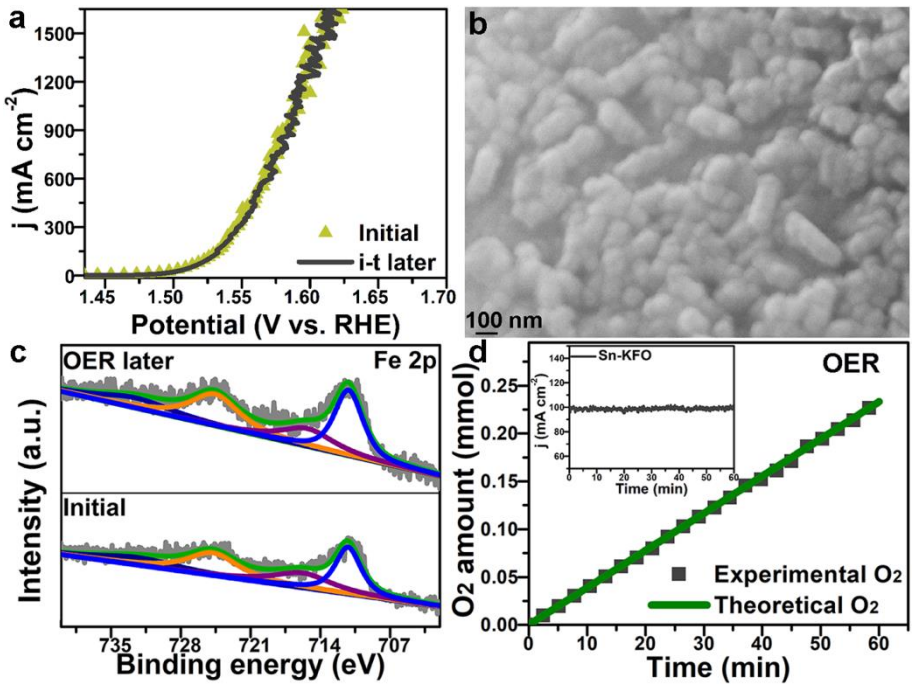


**Fig. S6**. The (a) LSV curve that i-t test later, (b) SEM image (c) Fe 2p spectra and (d) Faraday efficiency of Sn-KFO that after the OER course.

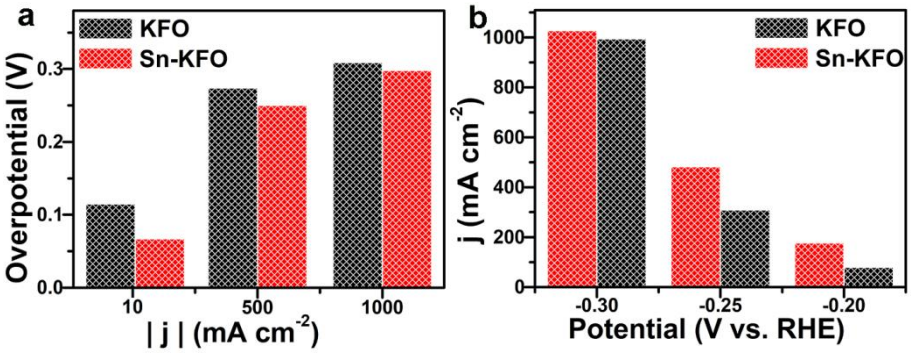


**Fig. S7.** (a, b) The bar-graphs between current density (j) and potential (V) of Sn-KFO and KFO during the HER process.

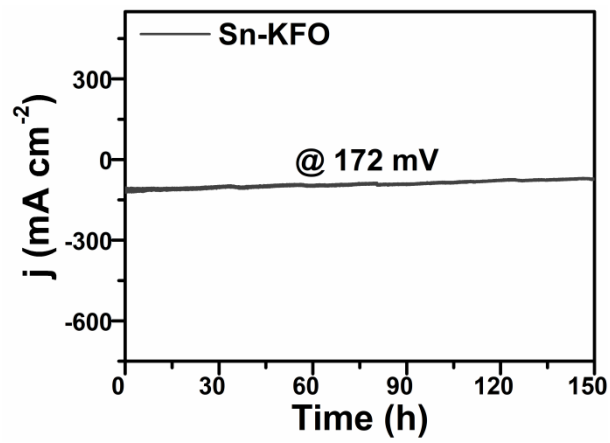


**Fig. S8.** The i-t curves of Sn-KFO for the HER course.

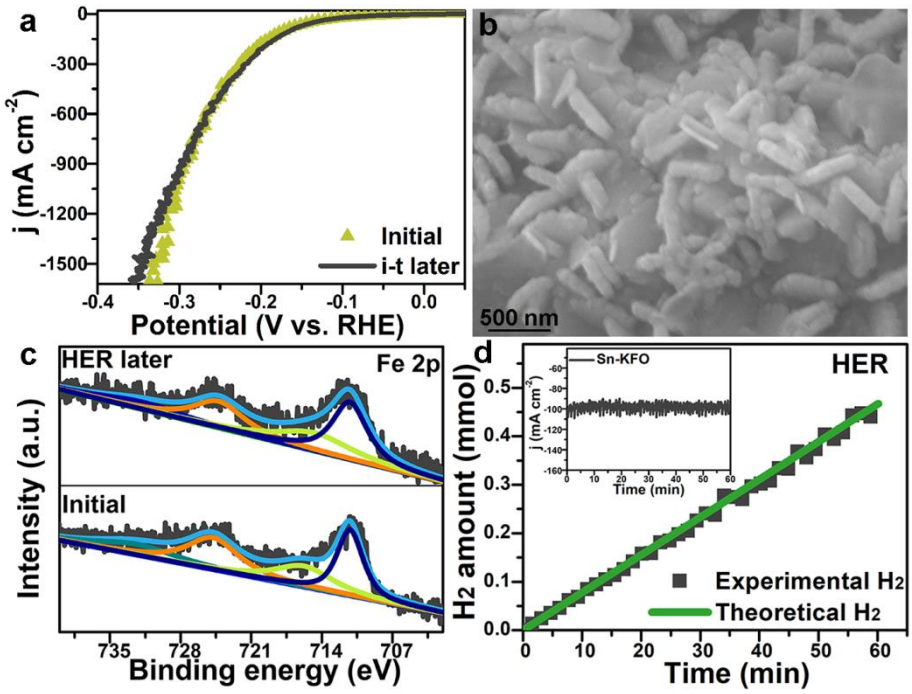


**Fig. S9**. The (a) LSV curve that i-t test later, (b) SEM image (c) Fe 2p spectra and (d) Faraday efficiency of Sn-KFO that after the OER course.

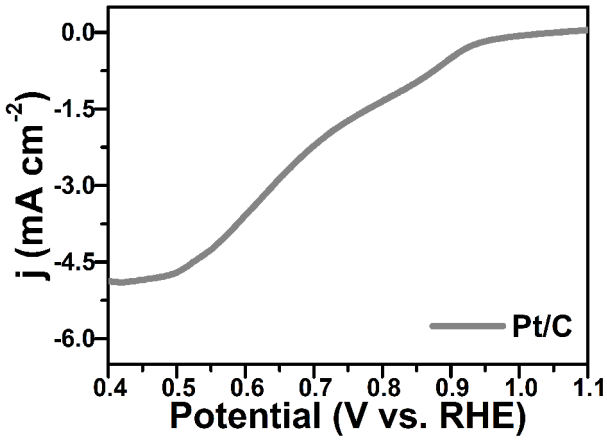


**Fig. S10**. The ORR plot of NF based Pt/C electrode.

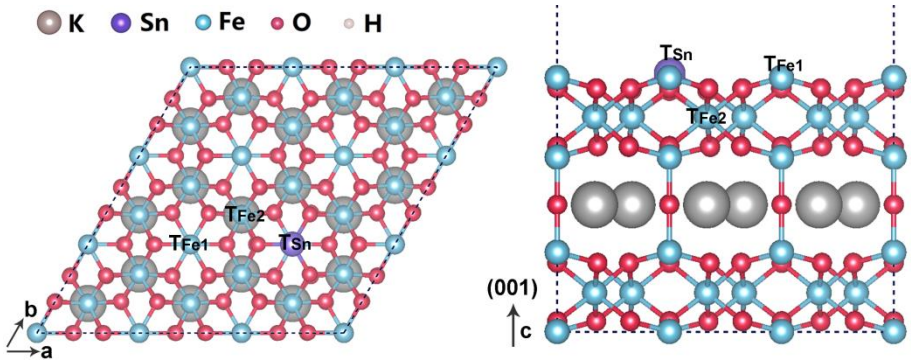


**Fig. S11**. The top and side views of the slab model corresponding to the (001) surface for the Sn-KFO system.

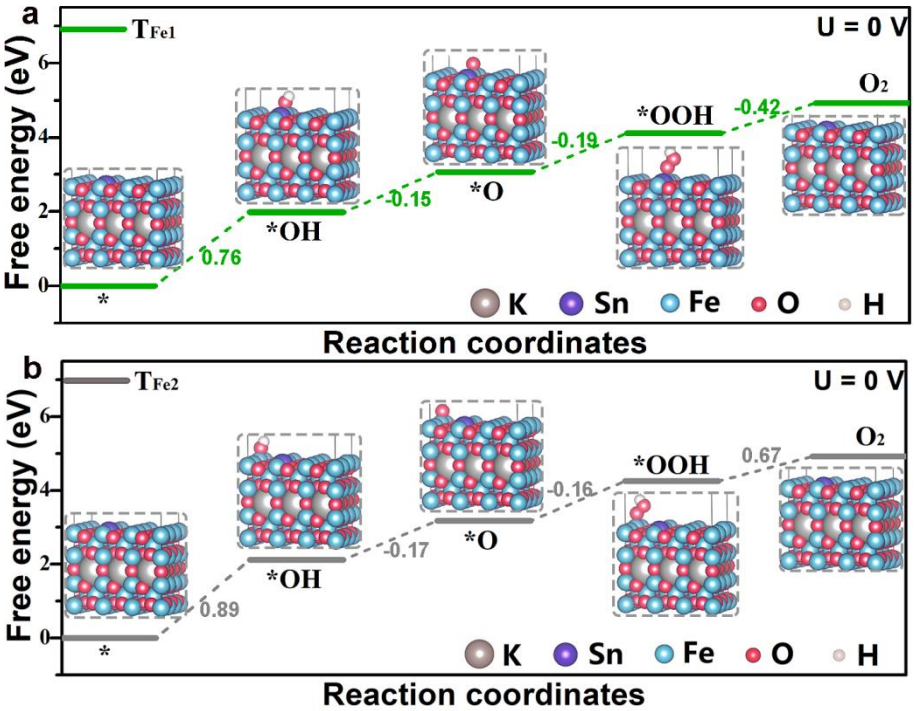


**Fig. S12.** The theory calculation at (a) $T_{Fe1}$ and (b) $T_{Fe2}$ site when U = 0, insert atomic structure diagrams are the corresponding absorptive state.

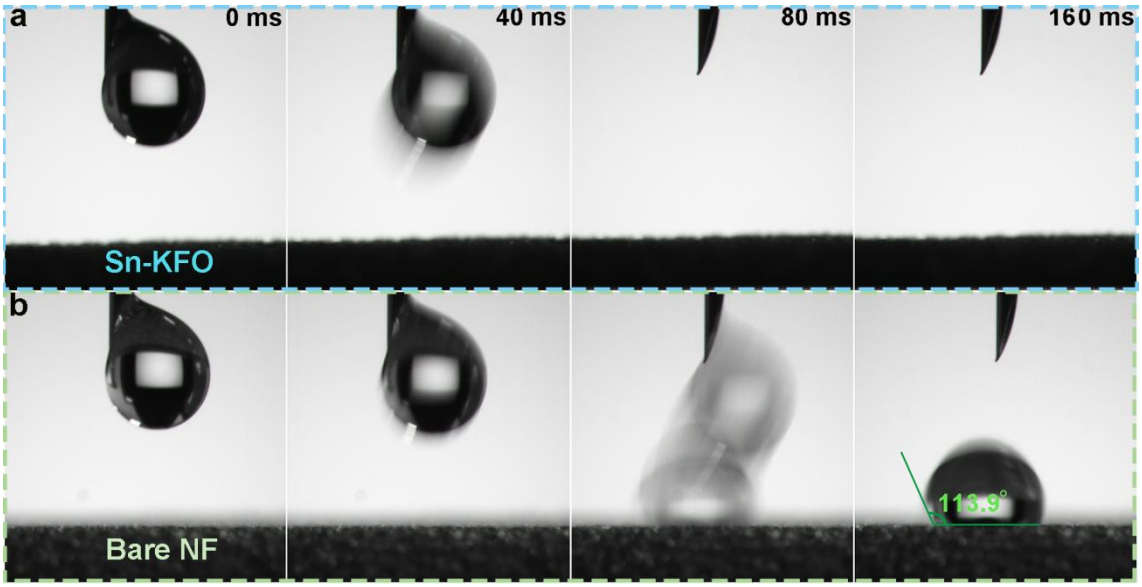


**Fig. S13**. Contact angel testing images of Sn-KFO and bare NF that at 0, 40, 80 and 160 ms after the water droplets come into contact with the surface of the material.

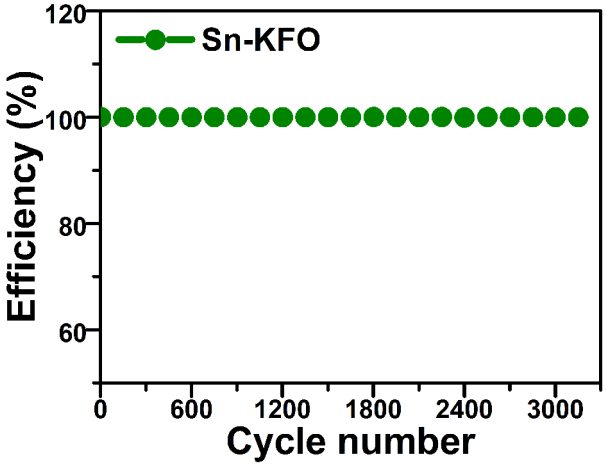


**Fig. S14**. The Coulombic efficiency of the Zn-air assembled with Sn-KFO serving as air-cathode, one cycle of charging-discharging needs 20 min at current density of 10 mA $cm^{-2}$.

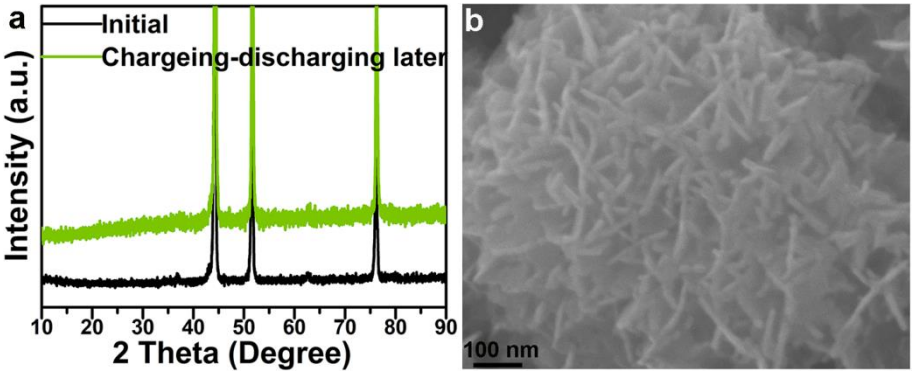


**Fig. S15**. (a) The XRD result and (b) SEM image of Sn-KFO that after the long-time charging and discharging process.

**Table S2**. A properties comparison of various electrocatalysts for overall water splitting (OWS).

| Catalys (OWS) | Voltage at 10 mA $cm^{-2}$ (V) | Voltage at 100 mA $cm^{-2}$ (V) | Reference |
|---|---|---|---|
| **Sn-KFO** | 1.55 | 1.70 | This work |
| **KFO** | 1.59 | 1.73 | This work |
| **Pt/C‖$RuO_2$** | 1.54 | 1.81 | This work |
| **Co/CNFs** | 1.60 | —— | [6] |
| **$Co_9S_8/Ni_3S_2$/NF** | 1.64 | —— | [7] |
| **CoMoO nanosheet arrays@NF** | 1.68 | ≈1.88 | [8] |
| **$Ni_3FeN$/r-GO** | 1.60 | ≈1.96 | [9] |
| **P-$Co_3O_4$/NF** | 1.63 | —— | [10] |
| **CoP@3D $Ti_3C_2$-Mxene** | 1.57 | ≈1.70 | [11] |

| | | | |
|---|---|---|---|
| **P-doped Co-Ni-S/NF** | 1.60 | —— | [12] |
| **$RuO_2$/NiO/NF** | 1.50 | —— | [13] |
| **Fe-$Ni_2P$** | 1.49 | ≈1.73 | [14] |
| **$Ni_3S_2$-NGQDs/NF** | 1.58 | —— | [15] |
| **NiFe/$Ni(OH)_2$/NiAl** | 1.59 | —— | [16] |
| **MoP/$Ni_2P$/NF** | 1.55 | —— | [17] |
| **N(P)-doped 304-type stainless steel mesh** | 1.74 | —— | [18] |
| **Cu@$CoS_x$/Cu Foam** | 1.50 | 1.80 | [19] |
| **CoFePO/NF** | 1.56 | ≈1.95 | [20] |
| **N-$Ni_3S_2$/ NF** | 1.48 | ≈1.83 | [21] |
| **$NiCo_2S_4$ nanowire arrays** | 1.63 | —— | [22] |
| **NiFeOOH** | —— | 1.49 | [23] |
| **CP/CTs/Co-S** | 1.74 | —— | [24] |
| **NiCoP** | 1.58 | ≈1.81 | [25] |
| **CoFeZr oxides/NF** | 1.63 | ≈1.80 | [26] |
| **$MoS_2$-$NiS_2$/NGF** | 1.64 | —— | [27] |
| **Ni-graphitic carbon (NGC)** | 1.64 | —— | [28] |
| **Mo-$Ni_3S_2$ nano-rods** | 1.53 | —— | [29] |
| **Ni@NC800/NF** | 1.60 | —— | [30] |
| **$Ni_{1-x}Fe_x$/NC/NF** | 1.58 | —— | [31] |
| **$MoO_3$/Ni-NiO** | 1.55 | —— | [32] |
| **Cu@CuS** | 1.52 | —— | [33] |

**Table S3**. A conclusion of the Zn-air battery activities for the recently reported self-powered trifunctional catalysts.

| Trifunctional catalyst | Voltage at 10 mA $cm^{-2}$ (OWS) | Battery voltage (V) | Power density (mW $cm^{-2}$) | Charging and discharging cycle time @ 10 mA $cm^{-2}$ (h) | Voltage gap (V) | Reference |
|---|---|---|---|---|---|---|
| **Sn-KFO** | **1.55** | **1.365** | **136.9** | **> 1000** | **0.817** | **This work** |
| **KFO** | 1.59 | 1.33 | 130.1 | 320 | 0.910 | This work |
| **Pt/C-$RuO_2$** | 1.54 | 1.35 | 95.4 | 170 | 0.881 | This work |
| **Pt@Fe-MOF** | 1.46 | 1.40 | 104 | 95 | -- | [34] |
| **NiCoP/NiO** | 1.71 | 1.43 | 84.5 | 113 | 0.84--0.86 | [35] |
| **Fe-NiCoP** | 1.60 | 1.40 | -- | 900 cycles @ 5 | -- | [36] |

| | | | | | | |
|---|---|---|---|---|---|---|
| | | | | mA $cm^{-2}$ | | |
| **Fe Doped MOF CoV@CoO nanoflakes** | 1.53 | 1.45 | 138 | 50 | 0.89 | [37] |
| **Co-MOF-800** | -- | 1.38 | 144 | 85 @ 1 mA $cm^{-2}$ | 0.46--0.58 | [38] |
| **Co@NCL** | 1.70 | 1.47 | 170 | 200 | 0.88 | [39] |
| **Co/N-CNF-800** | 1.80 | -- | -- | 50 | 1.39 | [40] |
| **Fe-Co-Ni MOF** | 1.60 | 1.42 | 161 | 120 @ 5 mA $cm^{-2}$ | 0.46--0.56 | [41] |
| **3%$IrO_x$/NCNT** | 1.52 | 1.5 | 59.3 | 120 @ 5 mA $cm^{-2}$ | 0.65 | [42] |
| **CoFe@NC/NCHNSs-700** | 1.66 | 1.49 | 184 | 50 | ~0.87 | [43] |
| **CoDNG900** | -- | 1.45 | 205.6 | 667 | 0.82 | [44] |
| **Pt/d-CoP/NPC** | 1.53 | 1.39 | 182.8 | 200 | ~1.05 | [45] |
| **MoCoP-NPC** | 1.65 | 1.50 | 175.2 | 300 | 0.47--0.5 | [46] |
| **$FeZn_4Co$@CNFs** | -- | 1.50 | 107.6 | 118 | ~0.87 | [47] |
| **Co-COP** | -- | 1.46 | 83.6 | -- | -- | [48] |
| **SC-$Cu_{SA}$-NC** | 1.58 | 1.48 | 124.9 | 120 | ~0.9 | [49] |
| **Fe-N-C/$FeP_x$/NPSC** | 1.57 | 1.49 | 216.9 | 93 | 0.87-0.96 | [50] |
| **$RuCoO_x$** | 1.54 | 1.54 | 160 | 1100 cycles @ 5 mA $cm^{-2}$ | ~0.86 | [51] |
| **RuCo/NPC** | 1.68 | 1.45 | 79.4 | 16.67 @ 2 mA $cm^{-2}$ | ~0.75 | [52] |
| **Re-$Ni_3S_2$/NG/NF** | 1.58 | 1.36 | 99 | 266 | ~0.88 | [53] |
| **NAC@$Co_3O_4$/NCNTs/CNF** | -- | 1.43 | 267.6 | 67 | 0.8--1.25 | [54] |
| **Pd-coated (CoFe/NCNTs)** | 1.60 | 1.48 | 261 | 50 | 0.69 | [55] |
| **CoP/$Co_3O_4$-fC-pPVP** | 1.58 | 1.49 | 154 | 727 @ 5 mA $cm^{-2}$ | ~0.75 | [56] |
| **CoFeN-NCNTs//CCM** | 1.63 | 1.46 | 145 | 445 | 0.76 | [57] |
| **B-$CoSe_2$@CoNi LDH HNA** | 1.58 | 1.41 | 181.5 | 70 @ 1 mA $cm^{-2}$ | ~0.8 | [58] |
| **NiCu-$MoS_2$** | 1.62 | 1.43 | 283 | 133 | 0.71-0.74 | [59] |
| **$FeSn_2$@$FeSnO_x$@S-N-C-900** | -- | 1.50 | 64.5 | 24 | 1.5 | [60] |
| **SnSb-NC** | -- | 1.58 | 195.8 | 1106 | ~1.3 | [61] |
| **$Sn_{x=0.15}$-$Ga_2O_3$** | -- | -- | 138 | 30 | 0.58 | [62] |

## 4. Reference


[1] Jian, J.; Yuan, L.; Qi, H.; Sun, X. J.; Zhang, L.; Li, H.; Yuan, H. M.; Feng, S. H. *ACS Appl. Mater. Inter.* **2018**, 10, 40568.

[2] Jian, J.; H. M. Yuan, and et al. *J. Mater. Chem. A* **2021**, 9, 7586-7593.

[3] Perdew, J. P.; Burke, K.; Ernzerhof, M. *Phys. Rev. Lett.* **1998**, 77, 3865.

[4] Blochl, P. E. *Phys. Rev. B* **1994**, 50, 17953.

[5] Nørskov, J. K.; Bligaard, T.; Logadottir, A.; Kitchin, J. R.; Chen, J.; Pandelov, S.; Stimming, U. *J. Electrochem. Soc.* **2005**, 152, J23.

[6] Yang, Z. K.; Zhao, C. M.; Qu, Y. T.; Zhou, H.; Zhou, F. Y.; Wang, J.; Wu, Y.; Li, Y. D. *Adv. Mater*. **2019**, 31, 1808043.

[7] Du, Feng.; Shi, L.; Zhang, Y. T.; Li, T.; Wang, J. L.; Wen, G. H.; Alsaedi, A.; Hayat, T.; Zhou, Y.; Zou, Z. G. *Appl. Catal., B* **2019**, 253, 246.

[8] Zhang, Y.; Shao, Q.; Long, S.; Huang, X. Q. *Nano Energy* **2018**, 45, 448.

[9] Gu, Y. Chen, S.; Ren, J.; Jia, Y.; Chen, C. M.; Komarneni, S.; Yang, D. J.; Yao, X. D. *ACS Nano* **2018**, 12, 245.

[10] Wang, Z. C.; Liu, H. L.; Ge, R. X.; Ren, X.; Ren, J.; Yang, D. J.; Zhang, L. X.; Sun, X. P. *ACS Catal*. **2018**, 8, 2236.

[11] Xiu, L. Y.; Wang, Z. Y.; Yu, M. Z.; Wu, X. H.; Qiu, J. S. *ACS Nano* **2018**, 12, 8017.

[12] Zhang, F. F.; Ge, Y. C.; Chu, H.; Dong, P.; Baines, R.; Pei, Y.; Ye, M. X.; Shen, J. F. *ACS Appl. Mater. Inter.* **2018**, 10, 7087.

[13] Liu, J. S.; Zheng, Y.; Jiao, Y.; Wang, Z. Y.; Lu, Z. G.; Vasileff, A.; Qiao, S. -Z. *Small* **2018**, 14, 1704073.

[14] Li, Y. J.; Zhang, H. C.; Jiang, M.; Zhang, Q.; He, P. L.; Sun, X. M. *Adv. Funct. Mater*. **2017**, 27, 1702513.

[15] Lv, J. J.; Zhao, J.; Fang, H.; Jiang, L. P.; Li, L. L.; Ma, J.; Zhu, J. J. *Small* **2017**, 13,1700264.

[16] Niu, S.; Jiang, W. -J.; Tang, T.; Zhang, Y.; Li, J. -H.; Hu J. -S. *Adv. Sci*. **2017**, 4, 1700084.

[17] Du, C. C.; Shang, M. X.; Mao J. X.; Song W. B. *J. Mater. Chem. A* **2017**, 5, 15940.

[18] Balogun, M. -S.; Qiu, W. T.; Huang, Y. C.; Yang, H.; Xu, R. M.; Zhao, W. X.; Li, G. -R.; Ji, H. B.; Tong, Y. X. *Adv. Mater*. **2017**, 1702095.

[19] Liu, Y. P.; Li, Q. J.; Si, R.; Li, G. -D.; Li, W.; Liu, D. -P.; Wang, D. J.; Sun, L.; Zhang, Y.; Zou, X. X. *Adv.Mater*. **2017**, 29, 1606200.

[20] Duan, J. J.; Chen, S.; Vasileff, A.; Qiao, S. Z. *ACS Nano* **2016**, 10, 8738

[21] Chen, P. Z.; Zhou, T. P.; Zhang, M. X.; Tong, Y.; Zhong, C. A.; Zhang, N.; Zhang, L. D.; Wu, C. Z.; Xie, Y. *Adv. Mater*. **2017**, 29, 1701584.

[22] Sivanantham, A.; Ganesan, P.; Shanmugam, S. *Adv. Funct. Mater*. **2016**, 26, 4661.

[23] Zhou, H. Q.; Yu, F.; Zhu, Q.; Sun, J. Y.; Qin, F.; Yu, L.; Bao, J. M.; Yu, Y.; Chen, S.; Ren, Z. F. *Energy Environ. Sci*. **2018**, 11, 2858.

[24] Wang, J.; Zhong, H. -X.; Wang, Z. -L.; Meng, F. -L.; Zhang, X. -B. *ACS Nano* **2016**, 10, 2342.

[25] Liang, H. F.; Gandi, A. N.; Anjum, D. H.; Wang, X. B.; Schwingenschlogl, U.; Alshareef, H. N. *Nano Lett.* **2016**, 16, 7718.

[26] Huang, L. L.; Chen, D. W.; Luo, G.; Lu, Y. -R.; Chen, C.; Zou, Y. Q.; Dong, C. -L.; Li, Y. F.; Wang, S. Y. *Adv. Mater*. **2019**, 1901439.

[27] Kuang, P. Y.; He, M.; Zou, H. Y.; Yu, J. G.; Fan, K. *Appl. Catal., B* **2019**, 254, 15.

[28] Zhou, B. H.; Zhang, M. C.; He, W. Y.; Wang, H. M.; Jian, M. Q.; Zhang, Y. Y. *Carbon* **2019**, 150, 21.

[29] Cui, Z.; Ge, Y. C.; Chu, H.; Baines, R.; Dong, P.; Tang, J. H.; Yang, Y.; Ajayan, P. M.; Ye, M. X.; Shen, J. F. *J. Mater. Chem. A*, **2017**, 5, 1595.

[30] Xu, Y.; Tu, W. G.; Zhang, B. W.; Yin, S. M.; Huang, Y. Z.; Kraft, M; Xu, R. *Adv. Mater*. **2017**, 29, 1605957.

[31] Zhang, X.; Xu, H. M.; Li, X. X.; Li, Y. Y.; Yang, T. B.; Liang, Y. Y. *ACS Catal*. **2016**, 6, 580.

[32] Li, X. P.; Wang, Y.; Wang, J. J.; Da, Y. M.; Zhang, J. F.; Li, L. L.; Zhong, C.; Deng, Y. D.; Han, X. P.; Hu, W. B. *Adv. Mater.* **2020**, 32, 2003414.

[33] Doan, T. L. L.; Tran, D. T.; Nguyen, D. C.; Kim, D. H.; Kim, N. H.; Lee, J. H. *Adv. Funct. Mater.* **2020**, 2007822.

[34] Wang, C.-P.; Bu, X.-H.; and et al. *Small* **2023**, 2305201.

[35] Hu, X. L.; Pan, F. S.; and et al. *Green Energy Environ.* **2023**, 8, 601-611.

[36] He, B.; Su, Z.; and et al. *CrystEngComm* **2021**, 23, 3861.

[37] Muthurasu, A.; Kim, H. Y.; and et al. *Nano Energy*, **2021**, 106238.

[38] Duan, X. D.; Zheng, H. G.; and et al. *J. Energy. Chem.* **2021**, 56, 290-298.

[39] Liu, Q.; Yang, W. Y. and et al. *Chemical Eng. J.* **2021**, 423, 130313.

[40] Liu, J.; Leung, K. H. and et al. *ACS Appl. Mater. Interfaces* **2022**, 14, 4399-4408.

[41] Farahani, F. S.; Mousavi, M. F.; and et al. *J. Am. Chem. Soc*. **2022**, 144, 15903-15906.

[42] Liu, N.; Guan, J. Q.; and et al. *Electrochimica Acta* **2021**, 380, 138215.

[43] Wang, S. J.; Hu, Y.; and et al. *Appl. Catal., B* **2021**, 298, 120512.

[44] Wang, A. S.; Wang, W. C.; and et al. *Appl. Catal., B* **2021**, 281, 119514.

[45] Wu, Z. X.; Wang, L.; and et al. *Chinese J. Catal.* **2023**, 46, 36-47.

[46] Zhao, S. L.; Zhu, Z. H.; and et al. *Small* **2023**, 2302414.

[47] Wang, F. L.; Chen, Y. L.; and et al. *J. Power Sources* **2022**, 521, 230925.

[48] Yao, Y.-F.; Xiao, X.-Y.; and et al. *Catal. Sci. Technol.* **2023**, 13, 6321-6330.

[49] Zhang, Y. L.; Guo, S. H.; and et al. Composites Part B **2023**, 253, 110575.

[50] Li, P.; Liu, S.; and et al. *Chemical Eng. J.* **2021**, 421, 129704.

[51] Zhou, C. H.; Zhang, R. F.; and et al. *Nano Lett.* **2021**, 21, 9633-9641.

[52] Pei, Y.; Wang, J. C.; and et al. *Chem. Commun.* **2021**, 57, 1498-1501.

[53] Han, X. T.; Li, N. N.; and et al. *Composites Part B* **2022**, 234, 109670.

[54] Yao, X. Y.; Zhang, W. M.; and et al. *Inorg. Chem. Front.* **2022**, 9, 2517-2529.

[55] Manjunatha, R.; Zhang, J. J.; and et al. *Green Energy Environ.* **2022**, 7, 933-947.

[56] Liu, Z.; Xu, W. J.; and et al. *Electrochimica Acta* **2022**, 412, 140134.

[57] Zhou, G. Z.; Wang, L.; and et al. *Adv. Funct. Mater.* **2021**, 2107608.

[58] Song, J. N.; Peng, S. J.; and et al. *Adv. Sci.* **2022**, 2104522.

[59] Kumar, M.; Nagaiah, T. C.; and et al. *J. Mater. Chem. A* **2023**, 11, 18336-18348.

[60] Zhang, X. Y.; Shan, Y. K.; and et al. *Electrochimica Acta* **2019**, 320.

[61] Li, S. T.; Yang, Q.; and et al. *Inorg. Chem. Front.* **2023**, 10, 3568-3576.

[62] Nair, A. N.; Sreenivasan, S. T.; *Small* **2022**, 18, 2202648.